

Doppler-Division Multiplexing for MIMO OFDM Joint Sensing and Communications

Oliver Lang, *Member, IEEE*, Christian Hofbauer, *Member, IEEE*, Reinhard Feger, and Mario Huemer, *Senior Member, IEEE*

Abstract—A promising waveform candidate for future joint sensing and communication systems is orthogonal frequency-division multiplexing (OFDM). For such systems, supporting multiple transmit antennas requires multiplexing methods for the generation of orthogonal transmit signals, where equidistant subcarrier interleaving (ESI) is the most popular multiplexing method. In this work, we analyze a multiplexing method called Doppler-division multiplexing (DDM). This method applies a phase shift from OFDM symbol to OFDM symbol to separate signals transmitted by different Tx antennas along the velocity axis of the range-Doppler map. While general properties of DDM for the task of radar sensing are analyzed in this work, the main focus lies on the implications of DDM on the communication task. It will be shown that for DDM, the channels observed in the communication receiver are heavily time-varying, preventing any meaningful transmission of data when not taken into account. In this work, a communication system designed to combat these time-varying channels is proposed, which includes methods for data estimation, synchronization, and channel estimation. Bit error ratio (BER) simulations demonstrate the superiority of this communications system compared to a system utilizing ESI.

Index Terms—Communication, multiplexing, OFDM.

I. INTRODUCTION

POTENTIAL applications of systems capable of joint sensing and communications include automotive car-to-car communications and cellular sensing [1]–[6]. While many different system architectures and waveform designs are possible, a so-called dual-function radar-communication system is assumed in this work that uses the very same transmit signals for both, radar sensing and communications, simultaneously. Further, it is assumed that the communica-

tion receiver and the radar receiver are located at different positions.

A prominent waveform for joint sensing and communication systems is orthogonal frequency-division multiplexing (OFDM) [7]–[17], which is also basis for the investigations in this work.

For many radar sensing applications, detecting the angular positions of objects in the sensor's vicinity is of importance. This is usually achieved by utilizing digital beamforming (DBF) in combination with several transmit (Tx) and receive (Rx) antennas. These so-called multiple-input multiple-output (MIMO) systems [18] employ multiplexing methods for generating orthogonal transmit signals that are separable in the receiver. The most popular multiplexing method for the OFDM waveform is equidistant subcarrier interleaving (ESI) [13], [19], for which each subcarrier is assigned to only one of the N_{Tx} Tx antennas (cf. Fig. 1 a). Hence, signals radiated by different Tx antennas can be separated in frequency domain. Several extensions of ESI exist with randomly allocated subcarriers [20], with non-equidistantly allocated subcarriers [15], and with dynamically allocated subcarriers [21]. The latter one is referred to as non-equidistant dynamic subcarrier interleaving (NeqDySI), and it changes the allocation of the subcarriers onto the Tx antennas from OFDM symbol to OFDM symbol.

A multiplexing method analyzed in [22] is denoted as auto-correlation-based code-division multiplexing (AC-CDM). For this method, the same data are radiated on every Tx antenna and on every subcarrier except for antenna-specific time delays. These time delays, which are implemented via linearly increasing phase rotations along the subcarriers, move the corresponding receive signals along the range axis of the range-Doppler map (RDM) such that N_{Tx} peaks appear along the range axis for each real object.

Another multiplexing method analyzed in [22] is denoted as modified repeated symbol CDM (MRS-CDM), which applies orthogonal Hadamard codes onto the OFDM symbols transmitted by different Tx antennas. In the receiver, N_{Tx} RDMs are evaluated separately, one for each Tx antenna. In every RDM there appears one main peak and $N_{Tx} - 1$ spurs along the velocity axis for each real object such that the maximum unambiguous velocity is reduced by a factor of N_{Tx} .

A discrete Fourier transform (DFT)-coded multiplexing

Oliver Lang is with the Institute of Signal Processing, Johannes Kepler University, Linz, Austria (e-mail: oliver.lang@jku.at).

Christian Hofbauer is with Silicon Austria Labs GmbH, Linz, Austria (e-mail: christian.hofbauer@silicon-austria.com).

Reinhard Feger is with the Institute for Communications Engineering and RF-Systems, Johannes Kepler University, Linz, Austria (e-mail: reinhard.feger@jku.at).

Mario Huemer is with the Institute of Signal Processing, Johannes Kepler University, Linz, Austria, and also with the JKU LIT SAL eSPML Lab, 4040 Linz, Austria (e-mail: mario.huemer@jku.at).

The work of Christian Hofbauer was supported by Silicon Austria Labs (SAL), owned by the Republic of Austria, the Styrian Business Promotion Agency (SFG), the federal state of Carinthia, the Upper Austrian Research (UAR), and the Austrian Association for the Electric and Electronics Industry (FEEL).

This work was supported by the "University SAL Labs" initiative of SAL and its Austrian partner universities for applied fundamental research for electronic based systems.

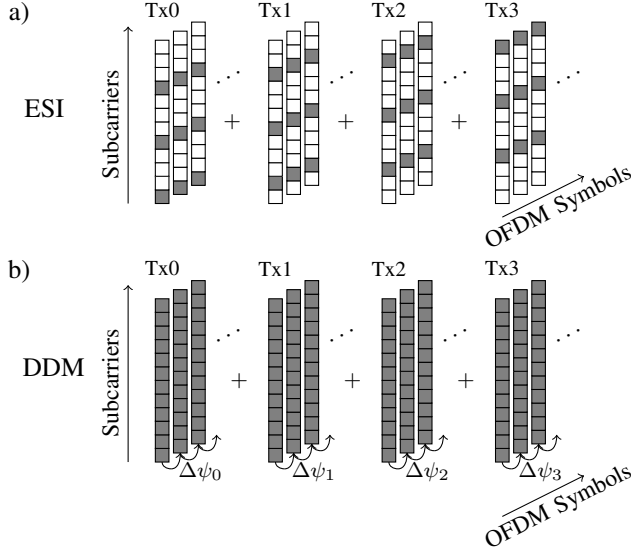


Fig. 1. a) Schematic visualization of the subcarrier allocation for ESI for the special case of 4 Tx antennas. Only every 4th subcarrier is active (gray blocks) for each Tx antenna. b) Sketch of the principle of DDM with unique phase shifts $\Delta\psi_k$ from OFDM symbol to OFDM symbol that shifts the received signals along the velocity axis. k denotes the Tx antenna index.

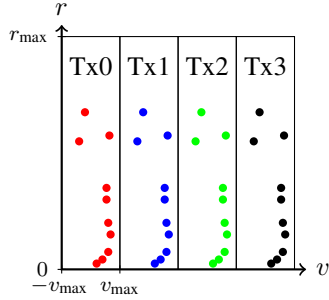


Fig. 2. Sketch of an RDM for DDM with $N_{Tx} = 4$ transmit antennas. Every real object results in N_{Tx} peaks in the RDM, each one associated with one Tx antenna.

method investigated in [23] applies a DFT matrix as precoding matrix onto the transmit signals that shifts the corresponding receive signals either along the range axis, the velocity axis, or both of them.

The multiplexing method analyzed in [24] is referred to as range-division multiplexing (RDMult), and it applies a phase shift from subcarrier to subcarrier to shift the signal components of the RDM along the range axis. The transmit signals generated by RDMult coincide with that generated by AC-CDM [22] and the DFT-coded multiplexing method [23] for special parametrization [24].

In this work, we analyze a multiplexing method referred to as Doppler-division multiplexing (DDM). DDM shares some similarities with the DFT-coded multiplexing method [23], with MRS-CDM [22], and with RDMult [24], however, there exist distinct differences in some details that will be discussed later. DDM modifies the transmit signal for each Tx antenna such that the received signal components are

shifted along the velocity axis. A proper modification to achieve this is a Tx antenna specific phase shift from OFDM symbol to OFDM symbol as indicated in Fig. 1 b). This phase shift is referred to as $\Delta\psi_k$, with the Tx antenna index $k = 0, 1, \dots, N_{Tx} - 1$. A schematic RDM for a MIMO OFDM radar system utilizing DDM is sketched in Fig. 2 for $N_{Tx} = 4$ Tx antennas. This figure shows a possible alignment of the Tx antennas and their corresponding signal components within the RDM. For radar sensing, the performance in terms of the signal-to-noise ratio (SNR) in the RDM of a MIMO OFDM radar system utilizing DDM is approximately equal to a MIMO OFDM radar system employing ESI, which is analyzed in this work.

DDM shares some similarities with the DFT-coded multiplexing method [23], which utilizes a DFT precoding matrix applied on the subcarriers and/or on the OFDM symbols to shift the signal components radiated by different Tx antennas either along the range axis, the velocity axis, or both of them. This DFT precoding matrix, when applied onto full OFDM symbols, corresponds to a phase shift from OFDM symbol to OFDM symbol as done for DDM. However, the design rule for choosing the phase shift utilized in this work differs from the one employed in [23] (cf. Sec. IV-A). Moreover, no analysis of the implications of the phase shift on the communication task was carried out in [23].

DDM also shares some similarities with MRS-CDM [22] by means of shifting signal components from different Tx antennas along the velocity axis. However, for MRS-CDM, each Tx antenna repeatedly transmits the same OFDM symbol during a whole frame of N_{sym} OFDM symbols, preventing efficient communications. In contrast to that, DDM allows for efficient communications as will be demonstrated in this work. Moreover, the orthogonal Hadamard codes applied on the transmit OFDM symbols for MRS-CDM in general differ from the phase shift utilized in DDM (cf. Sec. IV-A).

The multiplexing methods RDMult and DDM share some similarities, too. Both methods modify the transmit signals such that the corresponding received signals appear in different areas within the RDM. However, they have the following differences (with a detailed explanation later in this work)

- RDMult applies a phase shift from subcarrier to subcarrier, DDM applies a phase shift from OFDM symbol to OFDM symbol.
- For RDMult, the effective communication channel shows a repetitive pattern with constructive/destructive interferences along the subcarriers, while the effective communication channel for DDM shows a repetitive pattern with constructive/destructive interferences along the OFDM symbols.
- Both approaches add additional data redundancy to surpass the issue of the mentioned interferences. This is done by transmitting the same information over several subcarriers for RDMult, and by transmitting the same information over several OFDM symbols for DDM.
- Naturally, these different approaches of adding addi-

tional redundancy require different methods for synchronization, channel estimation, and data estimation.

As already mentioned, this work considers so-called dual-function radar-communication systems that use the very same transmit signals for both, the radar sensing task and the communication task, simultaneously. For the latter task, the specific design of the transmit signal for DDM affects the observed channel between transmitter and communication receiver. More specifically, it will turn out that the received signals at the communication receiver are affected by constructive or destructive interference, which is a typical effect for MIMO systems. However, the special transmit signals for DDM cause this interference to be heavily time-varying. As a consequence, the channel coefficients may significantly change in magnitude and phase from one OFDM symbol to the next one. Based on a comprehensive analysis of this observation, a communication system capable of dealing with these time-varying channels is proposed in this work, which includes adequate methods for synchronization, channel estimation, and data estimation. The communication system's performance is evaluated via extensive bit error ratio (BER) simulations.

Organization:

Sec. II introduces the general OFDM waveform and the usual radar receiver signal processing. The DDM method is described in Sec. III and discussed in the context of radar sensing and compared to competitive multiplexing methods in Sec. IV. The proposed communication system for a DDM OFDM waveform is explained in Sec. V, and Sec. VI analyzes the BER simulation results of this system. This work is concluded in Sec. VII.

Notation:

Vectors and matrices are indicated by lower-case and upper-case bold face variables, respectively. The element of a matrix at its l th row and k th column is defined as $[\mathbf{A}]_{l,k}$, where the indices start with 0. \mathbb{R} and \mathbb{C} represent the set of real and complex values, respectively. A superscript to \mathbb{R} or \mathbb{C} indicates the dimensions. Moreover, we use j represents the imaginary unit, $(\cdot)^T$ denotes the transposition, $(\cdot)^H$ represents the conjugate transposition, $(\cdot)^*$ indicates complex conjugation. The identity matrix of size $n \times n$ is denoted as \mathbf{I}^n , and a column vector of length n with all elements equal to 1 is indicated by $\mathbf{1}^n$. The Hadamard product and Hadamard division are represented by \odot and \oslash , respectively.

Definitions:

\mathbf{F}_N represents the DFT matrix of size $N \times N$ with $[\mathbf{F}_N]_{l,k} = \exp(-j2\pi lk/N)$ and $l, k = 0, \dots, N-1$. The vector $\mathbf{d}_N(f) \in \mathbb{C}^N$ is defined as

$$\mathbf{d}_N(f) = [1 \quad e^{j2\pi f} \quad \dots \quad e^{j2\pi f(N-1)}]^T, \quad (1)$$

with f being a unitless place-holder variable. The matrix $\mathbf{D}_N(f) \in \mathbb{C}^{N \times N}$ is a diagonal matrix defined as $\mathbf{D}_N(f) =$

TABLE I
PARAMETER DEFINITIONS.

Parameter	Symbol
Carrier frequency	f_c
Bandwidth	B
Number of subcarriers	N_c
ADC sampling time	$T_s = 1/B$
Subcarrier spacing	$\Delta f = B/N_c$
Length of an OFDM symbol	$T = 1/\Delta f$
Length of the cyclic prefix	T_{cp}
Number of OFDM symbols	N_{sym}
Number of Rx antennas	N_{Rx}
Number of Tx antennas	N_{Tx}

$\text{diag}(\mathbf{d}_N(f))$. Let $\mathbf{W}_N = \text{diag}(\mathbf{w}_N) \in \mathbb{R}^{N \times N}$ be a diagonal matrix containing the window function $\mathbf{w}_N \in \mathbb{R}^N$, then the windowed DFT of the complex-valued oscillation in $\mathbf{d}_N(f)$ yields [16]

$$\mathbf{u}_N(f) = \mathbf{F}_N \mathbf{W}_N \mathbf{d}_N(f) \quad (2)$$

$$= \begin{bmatrix} \sum_{n=0}^{N-1} [\mathbf{w}_N]_n e^{j2\pi(f - \frac{0}{N})n} \\ \vdots \\ \sum_{n=0}^{N-1} [\mathbf{w}_N]_n e^{j2\pi(f - \frac{N-1}{N})n} \end{bmatrix} \in \mathbb{C}^N. \quad (3)$$

The vector $\mathbf{u}_N(f)$ contains a main peak whose position within the vector is determined by f . The remaining elements of $\mathbf{u}_N(f)$ contain either zeros or sidelobes of the main peak.

II. BASICS OF OFDM RADAR

This section starts with a very brief textual explanation of the receiver signal processing chain of an OFDM-based single-input single-output (SISO) radar system, which corresponds to that used for DDM later in this work. After that, the signal model for the MIMO case is briefly described. The reader is referred to [9], [11]–[14], [16], [24] for more details.

A. OFDM Waveform and Radar Signal Processing

OFDM waveforms utilized in radar applications are typically based on the cyclic prefix (CP)-OFDM waveform. CP-OFDM is widely adopted in wireless communications [25] and the reader is thus expected to be familiar with it. Tab. I lists important design parameters of the OFDM waveform.

Fig. 3 visualizes the principle SISO OFDM radar signal processing chain. In this figure, matrix $\mathbf{S} \in \mathbb{C}^{N_c \times N_{\text{sym}}}$ contains the complex-valued amplitudes for all N_c subcarriers and for all N_{sym} OFDM symbols. The elements of \mathbf{S} are referred to as subcarrier symbols. The OFDM symbols are transformed into time domain, extended by a CP to avoid inter-symbol interference (ISI) [25], and radiated by the Tx antenna.

The receiver senses signals reflected from objects and feeds them into the radar receiver signal processing chain, which consists of the following steps:

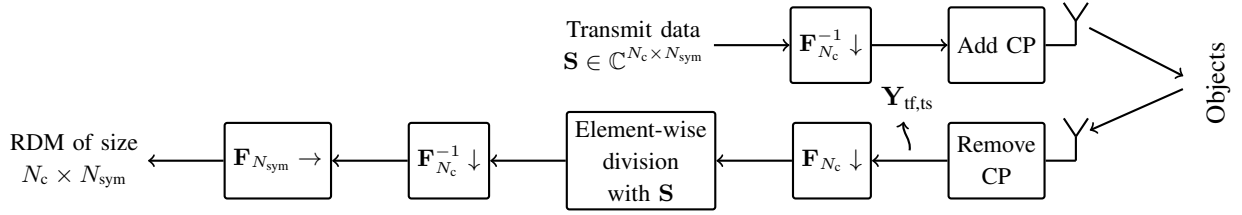


Fig. 3. SISO OFDM radar signal processing chain, where the parallel-to-serial conversion, the ADC and DAC, and the analog front-end are not shown for simplicity. The arrows \downarrow / \rightarrow represent the dimension of a matrix on which the operation is applied. Figure taken from [24].

- 1) Removing the CP.
- 2) Applying a DFT to obtain the received frequency domain OFDM symbols.
- 3) Performing an element-wise division by the transmitted subcarrier symbols in S .
- 4) Applying the so-called range inverse discrete Fourier transform (IDFT) unveils the range information.
- 5) Finally, the RDM of size $N_c \times N_{sym}$ is obtained after the so-called Doppler DFT.

With c_0 denoting the speed of light, the final RDM is determined by the values [9], [24], [26]

$$\Delta r = \frac{c_0}{2B} \quad \Delta v = \frac{c_0}{2f_c N_{sym} (T + T_{cp})} \quad (4)$$

$$r_{\max} = \Delta r N_c \quad v_{\max} = \pm \Delta v \frac{N_{sym}}{2}. \quad (5)$$

B. MIMO Signal Model

This section briefly recaps the complex baseband representation of the MIMO signal model from [24] since it is essential for deriving the DDM method. A detailed derivation can be found in [24], which itself is based on a SISO signal model derived in [16]. The derivation of the signal model considers only a single Rx antenna, while a possible extension to multiple Rx antennas can be easily adapted. At first, some definitions and assumptions are introduced.

Let the matrices $S_k \in \mathbb{C}^{N_c \times N_{sym}}$ with $k = 0, 1, \dots, N_{Tx} - 1$ contain the transmit subcarrier symbols for all Tx antennas. Each column of S_k represents one frequency domain OFDM symbol. The transmit signals in complex baseband can be derived by transforming these OFDM symbols into time domain and extending them with a CP.

The channel between transmitter and receiver assumes N_{path} propagation paths between each of the N_{Tx} Tx antennas and the Rx antenna with $r_{i,k}$ denoting the propagation distance for the k th Tx antenna along the i th path. $\tau_{i,k} = 2r_{i,k}/c_0$ is the corresponding round-trip delay time and can be normalized to $\bar{\tau}_{i,k} = \tau_{i,k}\Delta f$. $a_i \in \mathbb{C}$ models assumed constant amplitude and phase changes during propagation along the i th path [16].

At the receiver, the time domain analog-to-digital converter (ADC) samples are stored in a matrix $Y_{tf,ts} \in \mathbb{C}^{N_c \times N_{sym}}$, where every column corresponds to a received

OFDM symbol in time domain and without the CP. This matrix $Y_{tf,ts}$ is given by [24]

$$Y_{tf,ts} = \sum_{k=0}^{N_{Tx}-1} \sum_{i=0}^{N_{path}-1} \bar{a}_{i,k} \mathbf{D}_{N_c} \left(\frac{\bar{f}_{D_i}}{N_c} \right) \mathbf{F}_{N_c}^{-1} \mathbf{D}_{N_c}^* (\bar{\tau}_{i,k}) \cdot S_k \mathbf{D}_{N_{sym}} (\bar{f}_{D_i} \alpha). \quad (6)$$

where additive measurement noise is neglected, and where 'tf' and 'ts' indicate the fast time and the slow time over the vertical and horizontal matrix dimension, respectively. Additionally, we used $\bar{a}_{i,k} = a_i \exp(-j2\pi f_c \tau_{i,k}) \in \mathbb{C}$ and $\alpha = (T + T_{cp})/T \in \mathbb{R}$. The Doppler shift along the i th path caused by a relative velocity v_i is defined as $f_{D_i} = -2v_i f_c / c_0$, and it is normalized to $\bar{f}_{D_i} = f_{D_i} / \Delta f$. The implications of the Doppler shift are considered in form of a common phase error (CPE) and inter-carrier interference (ICI) affecting the received OFDM symbols. The CPE and ICI are represented in (6) in form of $\mathbf{D}_{N_{sym}}(\bar{f}_{D_i} \alpha)$ and $\mathbf{D}_{N_c} \left(\frac{\bar{f}_{D_i}}{N_c} \right)$, respectively.

For reasons of compactness of the subsequent mathematical derivations, we approximate the ICI term as $\mathbf{D}_{N_c} \left(\frac{\bar{f}_{D_i}}{N_c} \right) \approx \mathbf{I}^{N_c}$, which is valid for moderate v_i and sufficiently large Δf , leading to

$$Y_{tf,ts} = \sum_{k=0}^{N_{Tx}-1} \sum_{i=0}^{N_{path}-1} \bar{a}_{i,k} \mathbf{F}_{N_c}^{-1} \mathbf{D}_{N_c}^* (\bar{\tau}_{i,k}) S_k \mathbf{D}_{N_{sym}} (\bar{f}_{D_i} \alpha). \quad (7)$$

However, ICI as well as additive measurement noise are fully considered for all simulations in this work unless clearly stated otherwise.

In case several Rx antennas are considered, a similar matrix as in (7) can be constructed for every Rx antenna with appropriately modified parameters $\bar{a}_{i,k}$ and $\bar{\tau}_{i,k}$ [24].

III. DOPPLER-DIVISION MULTIPLEXING

The key aspect of DDM is a modification of the individual transmit signals for every Tx antenna such that the corresponding receive signals are shifted along the velocity axis in the RDM. These modified transmit signals as well as the resulting RDM are derived in the following.

The derivation begins with the MIMO signal model in (7). A shift along the velocity axis in the RDM is implemented by applying a phase shift from OFDM symbol to OFDM symbol. This phase shift is denoted as $\Delta\psi_k$ for

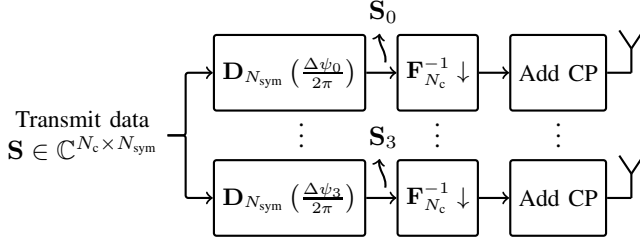


Fig. 4. DDM signal processing chain in the transmitter for the case of $N_{Tx} = 4$. The parallel-to-serial conversion, the DAC, and the analog front-end are not shown for simplicity.

$0 \leq k < N_{Tx}$. For instance, the first OFDM symbol of the k th Tx antenna remains unchanged, while the follow-up OFDM symbols are rotated in phase by $\Delta\psi_k$, $2\Delta\psi_k$, and so on.

Applying this phase shift in the transmitter is achieved by choosing \mathbf{S}_k in (7) to be

$$\mathbf{S}_k = \mathbf{S} \mathbf{D}_{N_{sym}} \left(\frac{\Delta\psi_k}{2\pi} \right), \quad (8)$$

cf. Fig. 4. Note that \mathbf{S} , and thus the payload, is the same for all Tx antennas. Only the modulation by $\mathbf{D}_{N_{sym}} \left(\frac{\Delta\psi_k}{2\pi} \right)$ makes them distinguishable among each other.

The time domain OFDM symbols at the k th Tx antenna in complex baseband are obtained by transforming the OFDM symbols in (8) into time domain and extending them by a CP.

The receive signal in complex baseband representation and after removing the CP is transformed into frequency domain by applying the DFT on the columns of $\mathbf{Y}_{f,ts}$, yielding

$$\begin{aligned} \mathbf{Y}_{f,ts} &= \mathbf{F}_{N_c} \mathbf{Y}_{t,ts} \\ &= \sum_{k=0}^{N_{Tx}-1} \sum_{i=0}^{N_{path}-1} \bar{a}_{i,k} \mathbf{D}_{N_c}^* (\bar{\tau}_{i,k}) \mathbf{S} \mathbf{D}_{N_{sym}} \left(\frac{\Delta\psi_k}{2\pi} + \bar{f}_{D_i} \alpha \right). \end{aligned} \quad (9)$$

(10)

The subscript 'f' indicates that the columns of $\mathbf{Y}_{f,ts}$ represent the frequency domain [16]. The second step is the Hadamard (element-wise) division with \mathbf{S} , yielding [24]

$$\mathbf{Z}_{f,ts} = \mathbf{Y}_{f,ts} \oslash \mathbf{S} \quad (11)$$

$$\begin{aligned} &= \sum_{k=0}^{N_{Tx}-1} \sum_{i=0}^{N_{path}-1} \bar{a}_{i,k} \mathbf{D}_{N_c}^* (\bar{\tau}_{i,k}) \mathbf{1}^{N_c} (\mathbf{1}^{N_{sym}})^T \\ &\quad \cdot \mathbf{D}_{N_{sym}} \left(\frac{\Delta\psi_k}{2\pi} + \bar{f}_{D_i} \alpha \right) \end{aligned} \quad (12)$$

$$= \sum_{k=0}^{N_{Tx}-1} \sum_{i=0}^{N_{path}-1} \bar{a}_{i,k} \mathbf{d}_{N_c}^* (\bar{\tau}_{i,k}) \mathbf{d}_{N_{sym}}^T \left(\frac{\Delta\psi_k}{2\pi} + \bar{f}_{D_i} \alpha \right). \quad (13)$$

The third step is applying the windowed range IDFT on the columns of $\mathbf{Z}_{f,ts}$ according to [16]

$$\mathbf{Z}_{r,ts} = \mathbf{F}_{N_c}^{-1} \mathbf{W}_{N_c} \mathbf{Z}_{f,ts} \quad (14)$$

$$= \sum_{k=0}^{N_{Tx}-1} \sum_{i=0}^{N_{path}-1} \bar{a}_{i,k} \mathbf{u}_{N_c}^* (\bar{\tau}_{i,k}) \mathbf{d}_{N_{sym}}^T \left(\frac{\Delta\psi_k}{2\pi} + \bar{f}_{D_i} \alpha \right). \quad (15)$$

The fourth processing step is applying the windowed Doppler DFT on the rows of $\mathbf{Z}_{r,ts}$, which yields

$$\mathbf{Z}_{r,v} = \mathbf{Z}_{r,ts} \mathbf{W}_{N_{sym}} \mathbf{F}_{N_{sym}} \quad (16)$$

$$= \sum_{k=0}^{N_{Tx}-1} \sum_{i=0}^{N_{path}-1} \bar{a}_{i,k} \mathbf{u}_{N_c}^* (\bar{\tau}_{i,k}) \mathbf{u}_{N_{sym}}^T \left(\frac{\Delta\psi_k}{2\pi} + \bar{f}_{D_i} \alpha \right). \quad (17)$$

This result represents the final RDM containing N_{Tx} peaks for every path i . These peaks are located at the same range but at different velocities.

IV. DISCUSSION OF DDM IN CONTEXT OF RADAR SENSING

A. Choice of $\Delta\psi_k$

The shift of the signal components along the velocity axis is determined by $\Delta\psi_k$. It is recommended to choose $\Delta\psi_k = 2\pi \frac{p}{N_{sym}}$ for any $p \in \mathbb{Z}$, which circularly shifts the corresponding signal components by p velocity bins without changing the magnitude or phase values. This statement can be proven by a straightforward modification of a related proof in [24, Appendix A]. Since no distortions of the magnitude or phase values are induced, a utilization of the them for DBF [4], [27], [28] is easily possible.

Furthermore, for $N_{Tx} = 4$, it is easy to prove that the choice $\Delta\psi_k = \{-\frac{3\pi}{4}, -\frac{1\pi}{4}, \frac{1\pi}{4}, \frac{3\pi}{4}\}$ separates the RDM in 4 equally sized areas, as sketched in Fig. 2, in which the bin representing zero relative velocity is located at the center of each area. Thus, it will be the primary choice for $\Delta\psi_k$ in this work.

We note that employing a DFT precoding matrix of size $N_{Tx} \times N_{Tx}$ as utilized in [23] may produce the same phase shift values as used in this work, however, it offers less freedom in choosing the shift along the velocity axis.

B. Maximum Unambiguous Range and Velocity

DDM provides the same unambiguous range r_{\max} as for a SISO OFDM radar system in (5). However, when dividing the velocity axis into N_{Tx} equally sized areas as discussed in Sec. IV-A, the maximum unambiguous velocity v_{\max} is decreased for DDM by a factor of N_{Tx} compared to the SISO case (cf. Fig. 2). As a consequence, the number of Tx antennas supported by DDM without further measures can be increased as long as no object violates the reduced maximum unambiguous velocity.

C. Beampattern

The beampattern is an important performance criterion for phased arrays and specifies the average signal power transmitted towards a certain direction. Simulations confirmed that the beampattern for DDM is almost uniform for practical values of N_{sym} .

D. Computational Complexity

The computational complexity required for adding the phase shift from OFDM symbol to OFDM symbol depends on $\Delta\psi_k$. In the worst case, $N_c N_{\text{sym}}$ phase rotations are required to apply the phase shift on every subcarrier in every OFDM symbol. For the special choice of $\Delta\psi_k = \{-\frac{3\pi}{4}, -\frac{1\pi}{4}, \frac{1\pi}{4}, \frac{3\pi}{4}\}$, the phase shifts are multiples of $\frac{\pi}{4}$ and thus computational complexity may be much lower. More specifically, if the symbol alphabet is symmetric with respect to rotations of $\frac{\pi}{4}$, applying $\Delta\psi_k$ can simply be implemented by modifying the so-called mapper with a time-dependent mapping function. For symbol alphabets without this symmetry, an extension of the alphabet might be considered.

E. Comparison with ESI

ESI has the following similarities and differences compared to DDM.

Processing gain: Since DDM activates every subcarrier on all Tx antennas, the processing gain follows as $G_p = N_{\text{sym}} N_c$. In contrast to that, ESI activates only every N_{Tx} th subcarrier per Tx antenna, leading to a reduced processing gain of $G_p = N_{\text{sym}} N_c / N_{\text{Tx}}$.

Average power per active subcarrier: Let ESI and DDM have the same average transmit power in order to provide a fair comparison. Then, as a consequence of the fewer activated subcarriers for ESI, the average power per active subcarrier is N_{Tx} times larger for ESI compared to DDM.

SNR in the RDM: Due to the same argumentation as provided in [24], the reduced power per active subcarrier and the increased processing gain cancel each other out. This results in approximately the same SNR in the RDM, and as a direct consequence, also the same SNR at the output of the DBF, for DDM as for ESI.

Maximum unambiguous range and velocity: As a consequence of the reduced number of active subcarriers per Tx antenna, ESI reduces r_{max} by a factor of N_{Tx} compared to a SISO OFDM system. In contrast to that, DDM offers the same r_{max} as a SISO OFDM system, but it reduces the unambiguous maximum velocity v_{max} by a factor of N_{Tx} .

F. Comparison with RDMult

RDMult in [24] shifts signal components along the range axis, and thus, reduces r_{max} by a factor of N_{Tx} compared to the SISO case. DDM shifts signal components along the velocity axis in the RDM, which entails a reduction of v_{max} by a factor of N_{Tx} compared the SISO case. Despite this difference, both multiplexing methods feature the same

TABLE II
WAVEFORM AND SYSTEM PARAMETERS.

Parameter	Value
Carrier frequency f_c	77 GHz
Bandwidth B	1 GHz
Number of subcarriers N_c	1024
ADC sampling time T_s	1 ns
Subcarrier spacing Δf	976.5 MHz
Length of an OFDM symbol T	1.024 μ s
Length of the cyclic prefix T_{cp}	1 μ s
Number of OFDM symbols N_{sym}	512
Number of Rx antennas N_{Rx}	1
Number of Tx antennas N_{Tx}	4
Symbol alphabet	QPSK
Phase shift $\Delta\psi_k$	$\{-\frac{3\pi}{4}, -\frac{1\pi}{4}, \frac{1\pi}{4}, \frac{3\pi}{4}\}$

average power per active subcarrier, the same processing gain, and the same SNR in the RDM.

V. COMMUNICATION SYSTEM BASED ON DDM

The DDM method generates transmit signals designed for multiplexing purposes in radar sensing applications. The effects of the transmit signal design due to DDM on the communication task are investigated in this section. Based on these investigations, a communication system specifically designed for DDM is proposed. In the following, the terms 'receiver' and 'Rx antenna' do not refer to the radar receiver but to the communication receiver.

This section begins with a discussion on different ways to represent the channel for DDM, followed by deriving the so-called 'effective' channel. This effective channel is a time-varying SISO channel that sufficiently describes the communication link between the transmitter and the communication receiver. After that, estimation methods for the effective channel and the transmit data are proposed. For these investigations, the waveform and system parameters are chosen according to Tab. II. The communication receiver employs only a single Rx antenna, which will turn out to be sufficient for enabling communications. An extension to multiple Rx antennas is straightforward at the cost of additional hardware and an increased power consumption for the communication receiver.

A. Channel Model

Fig. 5 shows the processing blocks for DDM in the transmitter, the N_{Tx} channel impulse responses (CIRs) from each Tx antenna to the Rx antenna, and the first two receiver processing blocks. On basis of that, we will introduce different channel representations

As for RDMult in [24], the channel for DDM can be represented in three possible ways.

1) *CIR Representation:* A straightforward way of describing the channel is to utilize the N_{Tx} individual CIRs. The model for these CIRs [29]–[31] and the model

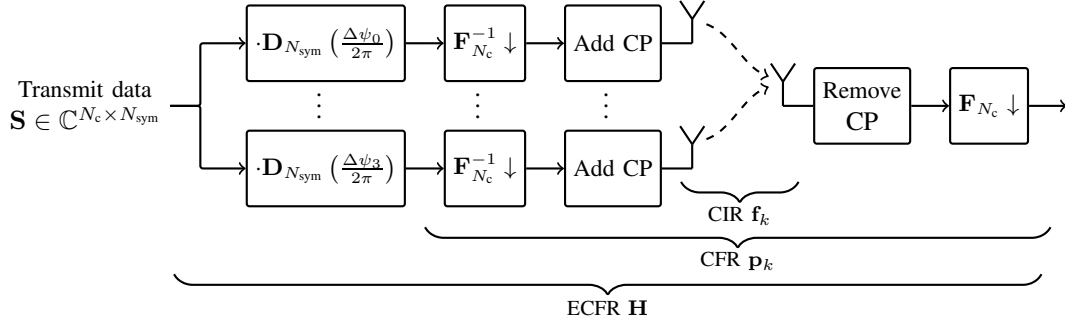


Fig. 5. Transmitter and receiver processing chains including the CIR, the CFR, and the ECFR with their covered processing blocks. The parallel-to-serial conversions, the DACs, the ADC, and the analog front-ends are not shown for simplicity. The figure is based on a similar figure in [24].

parametrization are equal to that employed in [24], such that a detailed description is omitted in this work. These CIRs are denoted as $\mathbf{f}_k \in \mathbb{C}^{N_f}$ for $0 \leq k < N_{Tx}$ and their assumed length is $N_f = 256$.

2) *CFR Representation*: Another way is to utilize the channel frequency responses (CFRs), which describe the N_{Tx} individual CIRs in frequency domain. These CFRs are denoted as $\mathbf{p}_k \in \mathbb{C}^{N_c}$ and are given by

$$\mathbf{p}_k = \mathbf{F}_{N_c} \mathbf{B}_{zp} \mathbf{f}_k, \quad (18)$$

where the matrix $\mathbf{B}_{zp} \in \mathbb{C}^{N_c \times N_f}$ zero-pads the CIRs \mathbf{f}_k to a length of N_c .

3) *ECFR Representation*: Here, we exploit the fact that all antennas transmit the same subcarrier symbols \mathbf{S} up to the deterministic phase shift $\Delta\psi_k$. Thus, the third way of describing the channel covers all shown processing blocks in Fig. 5. This channel representation is referred to as effective channel frequency response (ECFR), which can be modeled as a SISO channel despite the fact that several Tx antennas are involved.

The ECFR is mathematically described in the following. As depicted in Fig. 5, the ECFR covers the CFRs and the diagonal matrices $\mathbf{D}_{N_{sym}}(\frac{\Delta\psi_k}{2\pi})$. These diagonal matrices apply a phase shift from OFDM symbol to OFDM symbol. Thus, the ECFR will change from OFDM symbol to OFDM symbol. Let $\mathbf{H} \in \mathbb{C}^{N_c \times N_{sym}}$ denote the ECFR for all N_{sym} OFDM symbols, then, \mathbf{H} is given by

$$\mathbf{H} = \sum_{k=0}^{N_{Tx}-1} \mathbf{Q}_k, \quad (19)$$

where the matrices $\mathbf{Q}_k \in \mathbb{C}^{N_c \times N_{sym}}$ are given as

$$\mathbf{Q}_k = \mathbf{p}_k (\mathbf{1}_{N_{sym}})^T \mathbf{D}_{N_{sym}} \left(\frac{\Delta\psi_k}{2\pi} \right) \quad (20)$$

$$= \mathbf{p}_k \mathbf{d}_{N_{sym}} \left(\frac{\Delta\psi_k}{2\pi} \right)^T. \quad (21)$$

Each matrix \mathbf{Q}_k for $0 \leq k < N_{Tx}$ represents one signal path in Fig. 5.

4) *Properties of the ECFR*: Note that the N_{Tx} different terms used to construct the ECFR in (19) may interfere constructively or destructively. On top of that, this constructive/destructive interference turns out to be heavily time-varying.

The time-dependency of the ECFR can be well demonstrated for additive white Gaussian noise (AWGN) channels where \mathbf{Q}_k in (21) reduces to

$$\mathbf{Q}_k = \mathbf{1}^{N_c} \mathbf{d}_{N_{sym}} \left(\frac{\Delta\psi_k}{2\pi} \right)^T. \quad (22)$$

According to (22), all subcarriers experience the same effects. It is thus sufficient to inspect a single subcarrier, e.g., the first one.

This subcarrier is represented by the first row of \mathbf{Q}_k denoted as $[\mathbf{Q}_k]_{0,\mu}$, where the OFDM symbols are indexed with $0 \leq \mu < N_{sym}$. The magnitude and phase values for these elements are exemplarily sketched in form of arrows in the complex plane in Tab. III for the first 9 OFDM symbols $0 \leq \mu < 9$ and for the choice of $\Delta\psi_k = \{\frac{1\pi}{4}, \frac{3\pi}{4}, \frac{5\pi}{4}, \frac{7\pi}{4}\}$. According to (19), the sum of the elements $[\mathbf{Q}_k]_{0,\mu}$ for $0 \leq k < N_{Tx}$ yields the first subcarrier of the ECFR $[\mathbf{H}]_{0,\mu}$ for the μ th OFDM symbol, which is also sketched in Tab. III. One can see, that for $\mu = 0$ all components add up constructively. Hence, the ECFR can be considered to be good and the received signal power will be maximized for this OFDM symbol. The next three OFDM symbols observe destructive interference leading to full cancellation of the signal components, such that the received signal power is zero. For the OFDM symbols $\mu = 4, \dots, 7$ the arrows point in the opposite direction than for $\mu = 0, \dots, 3$, respectively. This pattern repeats for $\mu \geq 8$. For the AWGN case, we notice that constructive/destructive interference is observed with a period of 8 OFDM symbols. Within this period, the ECFR for the first 4 OFDM symbols equals that for the subsequent 4 OFDM symbols when inverting all signs.

The same analysis for the employed frequency selective channel model [24] is presented in the following. For this model, the magnitude values of $[\mathbf{H}]_{0,\mu}$ for an exemplary ECFR are shown in Fig. 6. Since the real-valued magnitude rather than the complex-valued amplitude values are shown, a period of 4 OFDM symbols is observed. Within these 4

The follow-up receiver signal processing is based on $\mathbf{z}_{\kappa,\gamma}$ rather than on $\mathbf{y}_{\kappa,\gamma}$, which allows describing the ECFR \mathbf{H} by only 4 columns. These 4 columns will be denoted as $\mathbf{h}_\gamma \in \mathbb{C}^{N_c}$ for $\gamma = 0, \dots, 3$. From now on, these 4 vectors are referred to ECFR for the sake of simplicity. A diagonal matrix with the ECFR is defined as $\mathbf{H}_\gamma = \text{diag}(\mathbf{h}_\gamma) \in \mathbb{C}^{N_c \times N_c}$.

The ECFR \mathbf{h}_γ transformed into the time domain is denoted as effective channel impulse response (ECIR) $\mathbf{g}_\gamma \in \mathbb{C}^{N_g}$, whose length N_g corresponds to the length of the CIR \mathbf{f}_k of $N_f = N_g = 256$. The ECIR and the ECFR are connected via

$$\mathbf{h}_\gamma = \mathbf{F}_{N_c} \mathbf{B}_{zp} \mathbf{g}_\gamma. \quad (30)$$

The introduced definitions and notations allow simplifying the model in (25)–(28) as

$$\mathbf{z}_{\kappa,\gamma} = \mathbf{H}_\gamma \mathbf{s}_{\kappa,\gamma} e^{j\varphi_{\kappa,\gamma}} + \mathbf{n}_{\kappa,\gamma} \quad (31)$$

$$= \mathbf{H}_\gamma \mathbf{x}_\kappa e^{j\varphi_{\kappa,\gamma}} + \mathbf{n}_{\kappa,\gamma}, \quad (32)$$

where $\mathbf{n}_{\kappa,\gamma} \in \mathbb{C}^{N_c}$ is a white Gaussian noise vector given by the DFT of the corresponding columns of \mathbf{N} . The alternating sign considered in (29) is ignored for the noise, since it does not affect its statistics. The covariance matrix of $\mathbf{n}_{\kappa,\gamma}$ is given by $\mathbf{C}_{nn} = N_c \sigma_n^2 \mathbf{I}^{N_c}$.

The matrix \mathbf{S} contains N_{pr} preamble OFDM symbols in the first N_{pr} columns, which are used for channel estimation later in this work. Thus, \mathbf{X} contains $N_{pr}/4$ preamble OFDM symbols in the first $N_{pr}/4$ columns, where it is assumed that N_{pr} is a multiple of 4. Let $\mathbf{x}_{pr} \in \mathbb{C}^{N_c}$ be the preamble OFDM symbol in frequency domain such that $\mathbf{x}_\kappa = \mathbf{x}_{pr}$ for $0 \leq \kappa < N_{pr}/4$.

For $\kappa \geq N_{pr}/4$, \mathbf{x}_κ consists of N_p pilot and N_d data subcarriers such that $N_c = N_p + N_d$. The symbols transmitted on the pilot subcarriers are known to the receiver and are used for synchronization. The variance of the assumed uncorrelated data subcarriers is denoted as σ_d^2 , which is usually normalized such that $\sigma_d^2 = 1$.

Dividing subcarriers into data subcarriers and pilot subcarriers not only applies to \mathbf{x}_κ but also to many other variables such as $\mathbf{s}_{\kappa,\gamma}$, $\mathbf{z}_{\kappa,\gamma}$, $\mathbf{n}_{\kappa,\gamma}$, \mathbf{h}_γ , and \mathbf{H}_γ . In the following, the superscript 'p' indicates the pilot subcarriers only, and the superscript 'd' refers the data subcarriers only. For instance, the sub-vector of $\mathbf{z}_{\kappa,\gamma}$ containing the pilot subcarriers only is denoted as $\mathbf{z}_{\kappa,\gamma}^p \in \mathbb{C}^{N_p}$, and the sub-vector containing the data subcarriers only is given by $\mathbf{z}_{\kappa,\gamma}^d \in \mathbb{C}^{N_d}$.

C. Channel Estimation

The OFDM preamble symbols are utilized for channel estimation. As a preparatory step, these symbols are synchronized to account for a potential CPE, e.g., caused by a relative velocity between transmitter and receiver. After that, the ECIR is estimated, which is then transformed into an estimate of the ECFR.

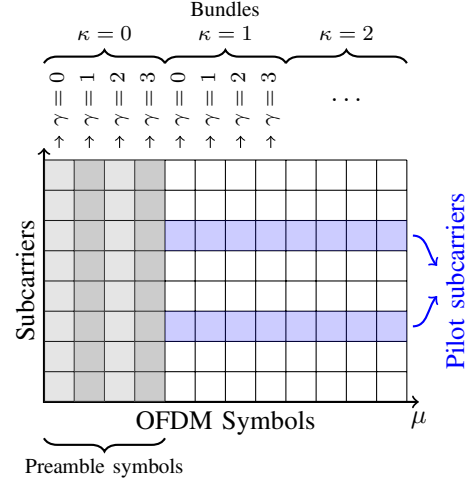


Fig. 7. Exemplary allocation of preamble OFDM symbols and pilot subcarriers in \mathbf{S} for DDM.

1) *Synchronization of the Preamble OFDM Symbols:* The model in (32) serves as a basis for synchronization, however, as usual in channel estimation, the roles of the channel and the preamble OFDM symbols are reversed. This yields

$$\mathbf{z}_{\kappa,\gamma} = \mathbf{X}_{pr} \mathbf{h}_\gamma e^{j\varphi_{\kappa,\gamma}} + \mathbf{n}_{\kappa,\gamma}, \quad (33)$$

where $\mathbf{X}_{pr} = \text{diag}(\mathbf{x}_{pr}) \in \mathbb{C}^{N_c \times N_c}$. Without loss of generality, $\varphi_{0,\gamma}$ is set to 0 and we estimate the CPE within $\mathbf{z}_{\kappa,\gamma}$ with respect to $\mathbf{z}_{0,\gamma}$ via [36]–[38]

$$\hat{\varphi}_{\kappa,\gamma} = \arg(\mathbf{z}_{0,\gamma}^H \mathbf{z}_{\kappa,\gamma}), \quad (34)$$

whereas $\hat{\cdot}$ indicates that $\hat{\varphi}_{\kappa,\gamma}$ is an estimate of $\varphi_{\kappa,\gamma}$. This estimation procedure is repeated for $0 \leq \gamma < 4$ and for $0 \leq \kappa < N_{pr}/4$. The estimated CPEs are then used to synchronize $\mathbf{z}_{\kappa,\gamma}$ according to

$$\tilde{\mathbf{z}}_{\kappa,\gamma} = \mathbf{z}_{\kappa,\gamma} \cdot e^{-j\hat{\varphi}_{\kappa,\gamma}}. \quad (35)$$

After synchronization, averaging within one bundle yields

$$\bar{\tilde{\mathbf{z}}}_\gamma = \frac{1}{N_{pr}/4} \sum_{\kappa=0}^{N_{pr}/4-1} \tilde{\mathbf{z}}_{\kappa,\gamma}. \quad (36)$$

With (30) and (36), (33) can be approximated by

$$\begin{aligned} \bar{\tilde{\mathbf{z}}}_\gamma &\approx \underbrace{\mathbf{X}_{pr} \mathbf{F}_{N_c} \mathbf{B}_{zp}}_{\mathbf{M}_{pr}} \mathbf{g}_\gamma + \underbrace{\frac{1}{N_{pr}/4} \sum_{\kappa=0}^{N_{pr}/4-1} \mathbf{n}_{\kappa,\gamma}}_{\mathbf{n}_\gamma} \\ &= \mathbf{M}_{pr} \mathbf{g}_\gamma + \mathbf{n}_\gamma, \end{aligned} \quad (37)$$

which is the basis for the following estimation procedure.

2) *ECIR/ECFR Estimation:* Employing the commonly used best linear unbiased estimator (BLUE) [39]–[42] on (38), an estimate of the ECIR \mathbf{g}_γ follows as

$$\hat{\mathbf{g}}_\gamma = (\mathbf{M}_{pr}^H \mathbf{M}_{pr})^{-1} \mathbf{M}_{pr}^H \bar{\tilde{\mathbf{z}}}_\gamma. \quad (39)$$

The estimated ECIRs in (39) can be transformed into an estimate of the corresponding ECFRs \mathbf{h}_γ via

$$\hat{\mathbf{h}}_\gamma = \mathbf{F}_{N_c} \mathbf{B}_{zp} \hat{\mathbf{g}}_\gamma. \quad (40)$$

The matrix representation of the estimate $\hat{\mathbf{h}}_\gamma$ is defined as $\hat{\mathbf{H}}_\gamma = \text{diag}(\hat{\mathbf{h}}_\gamma) \in \mathbb{C}^{N_c \times N_c}$. This procedure is repeated for all indexes $\gamma = 0, \dots, 3$.

D. Synchronization of OFDM Symbols for $\kappa \geq N_{pr}/4$

Considering only the pilot subcarriers of the model in (31) and replacing the ECFR by its estimate yields

$$\mathbf{z}_{\kappa,\gamma}^p \approx \hat{\mathbf{H}}_\gamma^p \underbrace{\mathbf{s}_{\kappa,\gamma}^p e^{j\varphi_{\kappa,\gamma}}}_{\mathbf{t}_{\kappa,\gamma}^p} + \mathbf{n}_{\kappa,\gamma}^p \quad (41)$$

$$= \hat{\mathbf{H}}_\gamma^p \mathbf{t}_{\kappa,\gamma}^p + \mathbf{n}_{\kappa,\gamma}^p, \quad (42)$$

where $\mathbf{t}_{\kappa,\gamma}^p = \mathbf{s}_{\kappa,\gamma}^p e^{j\varphi_{\kappa,\gamma}} \in \mathbb{C}^{N_p}$ represents CPE distorted pilot symbols [43], [44]. Employing the commonly used linear minimum mean square error (LMMSE) estimator [24], [36]–[39], [42], [45] on (42) yields

$$\hat{\mathbf{t}}_{\kappa,\gamma}^p = \left(\left(\hat{\mathbf{H}}_\gamma^p \right)^H \hat{\mathbf{H}}_\gamma^p + N_c \sigma_n^2 \mathbf{C}_{tt}^{-1} \right)^{-1} \left(\hat{\mathbf{H}}_\gamma^p \right)^H \mathbf{z}_{\kappa,\gamma}^p. \quad (43)$$

There, $\mathbf{C}_{tt} \in \mathbb{C}^{N_p \times N_p}$ denotes the covariance matrix of $\mathbf{t}_{\kappa,\gamma}^p$ and it is assumed to be a diagonal matrix for simplicity. The diagonal elements of \mathbf{C}_{tt} represent the pilot symbols' average power (averaged over the OFDM symbols). The estimate CPE distorted pilot symbols $\hat{\mathbf{t}}_{\kappa,\gamma}^p$ in (43) feature the error covariance matrix [37], [39], [42]

$$\mathbf{C}_{ee}^p = N_c \sigma_n^2 \left(\left(\hat{\mathbf{H}}_\gamma^p \right)^H \hat{\mathbf{H}}_\gamma^p + N_c \sigma_n^2 \mathbf{C}_{tt}^{-1} \right)^{-1}. \quad (44)$$

Comparing the estimates $\hat{\mathbf{t}}_{\kappa,\gamma}^p$ in (43) with the known transmitted pilot symbols $\mathbf{s}_{\kappa,\gamma}^p$ allows estimating the CPE for every $\kappa \geq N_{pr}/4$ and for $0 \leq \gamma < 4$ according to [36]–[38]

$$\hat{\varphi}_{\kappa,\gamma} = \arg \left(\left(\mathbf{s}_{\kappa,\gamma}^p \right)^H \mathbf{W} \hat{\mathbf{t}}_{\kappa,\gamma}^p \right). \quad (45)$$

Here, the diagonal matrix $\mathbf{W} \in \mathbb{C}^{N_p \times N_p}$ weights the estimated pilot subcarriers based on their estimation accuracy indicated by \mathbf{C}_{ee}^p in (44) [24], [37]. Finally, the estimated CPEs are used for de-rotating the received data subcarriers according to

$$\tilde{\mathbf{z}}_{\kappa,\gamma}^d = \mathbf{z}_{\kappa,\gamma}^d \cdot e^{-j\hat{\varphi}_{\kappa,\gamma}}. \quad (46)$$

E. Data Estimation

Recall that the same data symbols are transmitted over 4 consecutive OFDM symbols according to (23). Hence, the 4

vectors $\tilde{\mathbf{z}}_{\kappa,0}^d, \dots, \tilde{\mathbf{z}}_{\kappa,3}^d$ are used to estimate the data symbols in \mathbf{x}_κ^d . The connection between these vectors is given by

$$\underbrace{\begin{bmatrix} \tilde{\mathbf{z}}_{\kappa,0}^d \\ \tilde{\mathbf{z}}_{\kappa,1}^d \\ \tilde{\mathbf{z}}_{\kappa,2}^d \\ \tilde{\mathbf{z}}_{\kappa,3}^d \end{bmatrix}}_{\tilde{\mathbf{z}}_\kappa^d \in \mathbb{C}^{4N_d}} = \underbrace{\begin{bmatrix} \hat{\mathbf{H}}_0^d \\ \hat{\mathbf{H}}_1^d \\ \hat{\mathbf{H}}_2^d \\ \hat{\mathbf{H}}_3^d \end{bmatrix}}_{\hat{\mathbf{H}}^d \in \mathbb{C}^{4N_d \times N_d}} \mathbf{x}_\kappa^d + \underbrace{\begin{bmatrix} \mathbf{n}_{\kappa,0}^d \\ \mathbf{n}_{\kappa,1}^d \\ \mathbf{n}_{\kappa,2}^d \\ \mathbf{n}_{\kappa,3}^d \end{bmatrix}}_{\mathbf{n}_\kappa^d \in \mathbb{C}^{4N_d}} \quad (47)$$

$$\tilde{\mathbf{z}}_\kappa^d = \hat{\mathbf{H}}^d \mathbf{x}_\kappa^d + \mathbf{n}_\kappa^d. \quad (48)$$

The LMMSE estimator for \mathbf{x}_κ^d can be derived as [37], [39], [45]

$$\hat{\mathbf{x}}_\kappa^d = \left(\left(\hat{\mathbf{H}}^d \right)^H \hat{\mathbf{H}}^d + \frac{N_c \sigma_n^2}{\sigma_d^2} \mathbf{I}^{N_d} \right)^{-1} \left(\hat{\mathbf{H}}^d \right)^H \tilde{\mathbf{z}}_\kappa^d, \quad (49)$$

representing the final estimate of the data symbols.

VI. BER PERFORMANCE COMPARISON

In this section, the BER performance of the proposed MIMO OFDM system using DDM is compared with that of a SISO OFDM system and with that of MIMO OFDM systems utilizing ESI, RDMult, and NeqDySI investigated in [21]. For the latter one, it is assumed that the receiver knows the assignment of the subcarrier sets to the individual Tx antennas. All considered systems employ the system parameters listed in Tab. II except for the SISO OFDM system for which $N_{Tx} = 1$.

Additional processing blocks, e.g., the channel coder/decoder [37], [40], [46], the mapper/demapper [47]–[49], interleaver/deinterleaver, randomized CIR generation [29]–[31], correspond to those utilized in [24] such that a detailed description can be omitted in this work.

The simulations are carried out for fixed values of E_b/N_0 , where E_b is the average energy per bit of information, and where $N_0/2$ is the double-sided noise power spectral density of a bandpass noise signal [37]. To obtain the desired value of E_b/N_0 the noise variance σ_n^2 of the complex-valued AWGN at the receiver input is chosen according to [37], [50]

$$\sigma_n^2 = \frac{P_s}{(E_b/N_0)br\zeta\nu}. \quad (50)$$

There, P_s represents the average signal power per time-domain sample measured at the receiver input. Moreover, b is the number of bits per data symbol ($b = 2$ for quadrature phase-shift keying (QPSK)), r represents the code rate of the channel code, and $\zeta = N_c/(N_{cp} + N_c)$ accounts for the time domain samples in the CP. The parameter ν accounts for the additional redundancy discussed in Sec. V-A5. Thus, $\nu = \frac{1}{4}$ for the MIMO OFDM system employing DDM. RDMult adds a similar redundancy [24], such that $\nu = \frac{1}{4}$ is chosen also for the MIMO OFDM system utilizing RDMult. All other considered systems do not add any additional redundancy such that $\nu = 1$ is chosen for them. As a result, MIMO OFDM systems employing DDM and RDMult observe a higher noise variance σ_n^2 .

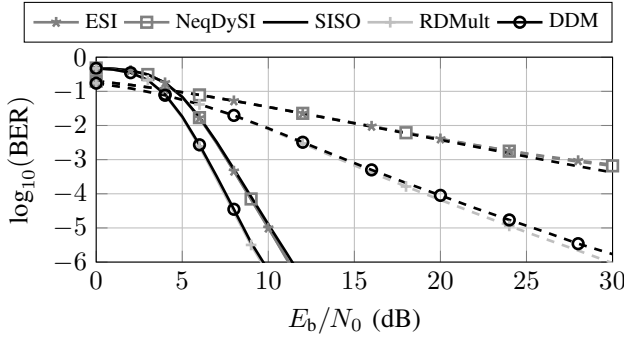


Fig. 8. BER curves for the case of perfect synchronization and perfect channel knowledge. The solid lines are for coded, and the dashed lines are for uncoded transmission.

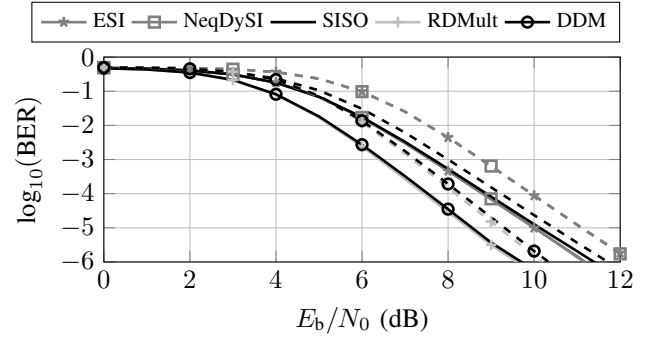


Fig. 9. BER curves for the case of perfect synchronization, code rate $r = 1/2$, and for perfect channel knowledge (solid) and for imperfect channel estimation (dashed).

The BER curves are simulated for three simulation scenarios detailed in the following.

1) *Perfect Channel Knowledge; Perfect Synchronization:*

In this first simulation, the receiver perfectly knows the channel between transmitter and receiver. The observed BER curves for uncoded and coded transmission are shown in Fig. 8. While for the uncoded case RDMult has a small advantage in BER performance over DDM, both systems feature approximately the same BER performance in the coded case and outperform the remaining systems by approximately 1.6 dB. This gain in BER performance is a result of the diversity gain elaborated on in Sec. V-A5.

As argued in [24], granting this diversity gain also to MIMO systems utilizing ESI and NeqDySI by means of adding additional redundancy would increase their BER performances as well at the cost of a reduced data rate.

The remaining simulations are shown for coded transmission only, since uncoded transmission is not relevant for real-world applications.

2) *Perfect Synchronization; Imperfect Channel Estimation based on Preamble OFDM Symbols:* Now, the channel is not perfectly known but rather estimated using the procedure derived in Sec. V-C. The channel estimation procedure for the SISO OFDM system is described in [37], [41]. The channels for the MIMO OFDM systems utilizing ESI and NeqDySI are estimated with the BLUE [39], [42], whose derivations are omitted in this work.

For a fair comparison by means of having the similar distortions on the channel estimates, all three systems shall have the same effective SNR for the averaged preamble OFDM symbols [24]. Hence, the increased noise variance σ_n^2 for the MIMO OFDM systems with DDM and RDMult is compensated by employing $N_{pr} = 16$ preamble OFDM symbols, while the other systems use $N_{pr} = 4$.

The resulting BER curves are shown in Fig. 9. This figure also visualizes the simulation results for the case of perfect channel knowledge from Fig. 8 as reference. While the MIMO systems are less prone to imperfect channel knowledge, the loss in performance for all three systems

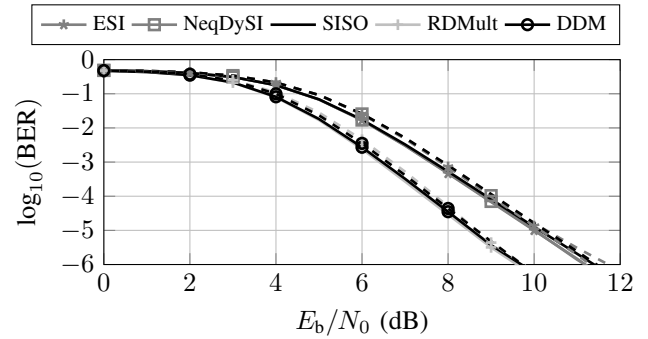


Fig. 10. BER curves for the case of perfect channel knowledge, code rate $r = 1/2$, and for perfect synchronization (solid) and for imperfect synchronization (dashed).

is moderate¹.

3) *Perfect Channel Knowledge; Imperfect Synchronization using Pilot Subcarriers:* Now, the channels are perfectly known, but the synchronization is performed using pilot subcarriers rather than having perfect synchronization. The SISO OFDM system and the MIMO OFDM systems utilizing ESI and NeqDySI employ $N_p = 16$ pilot subcarriers. The MIMO OFDM systems with DDM and RDMult employ $N_p = 64$ pilot subcarriers in order to ensure the same effective SNR as argued previously. The BER curves visualized in Fig. 10 show that the loss in BER performance is minor for all considered systems.

4) *Perfect Channel Knowledge; Perfect CPE Synchronization; Disabled ICI:* The loss in BER performance due to ICI-induced distortions is analyzed by disabling ICI, while the channel is assumed to be known and the CPE is compensated perfectly. The resulting BER curves in Fig. 11 indicate that the loss in BER performance is negligible for all considered multiplexing methods with the chosen parametrization.

¹We note that in practice, not only the ECIRs but also the underlying CIRs may become highly time-varying for the assumed relative velocity between ± 60 m/s. This may entail the necessity of more frequent channel estimation or advanced channel tracking algorithms, whose analysis is beyond the scope of this work.

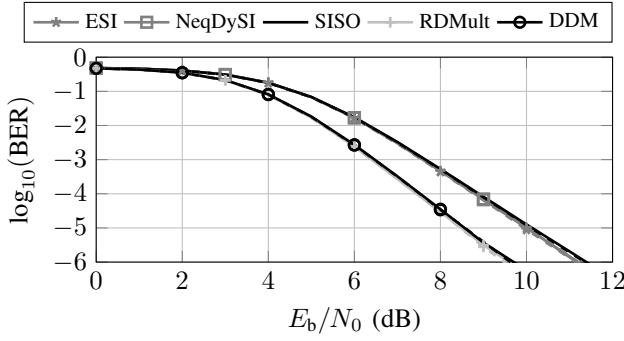


Fig. 11. BER curves for code rate $r = 1/2$, perfect synchronization and perfect channel knowledge. Simulation results are shown for activated (solid) and deactivated (dashed) ICI. The curves for DDM and RDMult as well as the curves for SISO, ESI and NeqDySI lie almost on top of each other.

VII. CONCLUSION

In this work, a novel MIMO OFDM joint radar and communication system designed for DDM was presented. This multiplexing method generates transmit signals that are separable along the velocity axis in the RDM. A thorough investigation of the properties of DDM for the radar sensing task and the communication task has been carried out in this work. For the radar sensing task, it turned out that DDM features the same SNR performance as RDMult and ESI. Differences between these multiplexing methods include

- the average power per active subcarrier,
- the processing gain, and
- the maximum unambiguous range and velocity.

The transmit signals generated by a MIMO OFDM system using DDM were analyzed for the communication task as well. We showed that a SISO channel sufficiently models the communication channel and that this SISO channel is heavily time-varying, entailing the necessity of counter measures. We proposed a communication system specifically designed to cope with the time-varying nature of the channel. This communication system includes methods for data estimation, synchronization, and channel estimation, whose performances were evaluated by means of BER simulations.

REFERENCES

- [1] O. B. Akan and M. Arik, "Internet of radars: Sensing versus sending with joint radar-communications," *IEEE Commun. Mag.*, vol. 58, no. 9, pp. 13–19, 2020.
- [2] D. Ma, N. Shlezinger, T. Huang, Y. Liu, and Y. C. Eldar, "Joint radar-communication strategies for autonomous vehicles: Combining two key automotive technologies," *IEEE Signal Process. Mag.*, vol. 37, no. 4, pp. 85–97, 2020.
- [3] C. Waldschmidt and H. Meinel, "Future trends and directions in radar concerning the application for autonomous driving," *Proc. Eur. Radar Conf.*, 2014, pp. 416–419.
- [4] M. Gerstmaier, A. Melzer, A. Onic, and M. Huemer, "On the Safe Road Toward Autonomous Driving: Phase Noise Monitoring in Radar Sensors for Functional Safety Compliance," *IEEE Signal Process. Mag.*, vol. 36, no. 5, pp. 60–70, 2019.
- [5] S. Sun, A. P. Petropulu, and H. V. Poor, "MIMO Radar for Advanced Driver-Assistance Systems and Autonomous Driving: Advantages and Challenges," *IEEE Signal Process. Mag.*, vol. 37, no. 4, pp. 98–117, 2020.

- [6] M. Gerstmaier, M. Gschwandtner, R. Findenig, A. Melzer, and M. Huemer, "Lego Radar Train — An Educational Workshop on Radar-based Advanced Driver Assistance Systems," *Proc. Eur. Signal Process. Conf.*, 2021, pp. 1981–1985.
- [7] N. Levanon, "Multifrequency complementary phase-coded radar signal," *IEE Proc. - Radar, Sonar Navigat.*, vol. 147, no. 6, pp. 276–284, 2000.
- [8] B. J. Donnet and I. D. Longstaff, "Combining MIMO Radar with OFDM Communications," *Proc. Eur. Radar Conf.*, 2006, pp. 37–40.
- [9] C. Sturm, E. Pancera, T. Zwick, and W. Wiesbeck, "A novel approach to OFDM radar processing," *Proc. IEEE Radar Conf.*, 2009, pp. 1–4.
- [10] D. Garmatyuk, J. Schuerger, Y. T. Morton, K. Binns, M. Durbin, and J. Kimani, "Feasibility study of a multi-carrier dual-use imaging radar and communication system," *Proc. Eur. Radar Conf.*, 2007, pp. 194–197.
- [11] C. Sturm, T. Zwick, and W. Wiesbeck, "An OFDM System Concept for Joint Radar and Communications Operations," *Proc. IEEE Veh. Technol. Conf.*, 2009, pp. 1–5.
- [12] C. Sturm, T. Zwick, W. Wiesbeck, and M. Braun, "Performance verification of symbol-based OFDM radar processing," *Proc. IEEE Radar Conf.*, 2010, pp. 60–63.
- [13] Y. L. Sit and T. Zwick, "Automotive MIMO OFDM radar: Subcarrier allocation techniques for multiple-user access and DOA estimation," *Proc. Eur. Radar Conf.*, 2014, pp. 153–156.
- [14] M. Braun, C. Sturm, A. Niethammer, and F. K. Jondral, "Parametrization of joint OFDM-based radar and communication systems for vehicular applications," *Proc. IEEE Int. Symp. Pers., Indoor, Mobile Radio Commun.*, 2009, pp. 3020–3024.
- [15] G. Hakobyan and B. Yang, "A novel OFDM-MIMO radar with non-equidistant subcarrier interleaving and compressed sensing," *Proc. Int. Radar Symp.*, 2016, pp. 1–5.
- [16] G. Hakobyan and B. Yang, "A Novel Inter-Carrier-Interference Free Signal Processing Scheme for OFDM Radar," *IEEE Trans. Veh. Technol.*, pp. 1–1, 2017.
- [17] O. Lang, R. Feger, C. Hofbauer, and M. Huemer, "OFDM Radar With Subcarrier Aliasing—Reducing the ADC Sampling Frequency Without Losing Range Resolution," *IEEE Trans. on Veh. Technol.*, vol. 71, no. 10, pp. 10 241–10 253, 2022.
- [18] B. Nuss, J. Mayer, and T. Zwick, "Limitations of MIMO and Multi-User Access for OFDM Radar in Automotive Applications," in *IEEE MTT-S Int. Conf. on Microw. for Intell. Mobility*, 2018, pp. 1–4.
- [19] C. Sturm, Y. L. Sit, M. Braun, and T. Zwick, "Spectrally interleaved multi-carrier signals for radar network applications and multi-input multi-output radar," *IET Radar, Sonar & Navig.*, vol. 7, no. 3, pp. 261–269, 2013.
- [20] C. Knill, F. Roos, B. Schweizer, D. Schindler, and C. Waldschmidt, "Random Multiplexing for an MIMO-OFDM Radar With Compressed Sensing-Based Reconstruction," *IEEE Microw. Wireless Compon. Lett.*, vol. 29, no. 4, pp. 300–302, 2019.
- [21] G. Hakobyan and B. Yang, "A novel OFDM-MIMO radar with non-equidistant dynamic subcarrier interleaving," *Proc. Eur. Radar Conf.*, 2016, pp. 45–48.
- [22] C. Knill, F. Embacher, B. Schweizer, S. Stephany, and C. Waldschmidt, "Coded OFDM Waveforms for MIMO Radars," *IEEE Trans. on Veh. Technol.*, 2021.
- [23] J. Suh, J. Lee, G.-T. Gil, and S. Hong, "Time-and-Frequency Hybrid Multiplexing for Flexible Ambiguity Controls of DFT-coded MIMO OFDM Radar," *IEEE Access*, vol. 9, 2021.
- [24] O. Lang, C. Hofbauer, R. Feger, and M. Huemer, "Range-Division Multiplexing for MIMO OFDM Joint Radar and Communications," *IEEE Trans. on Veh. Technol.*, pp. 1–15, 2022.
- [25] R. van Nee and R. Prasad, *OFDM for Wireless Multimedia Communications*, ser. Artech House universal personal communications library. Artech House, 2000.
- [26] O. Lang, A. Onic, C. Schmid, R. Feger, and M. Huemer, "Reducing Hardware Requirements and Computational Effort for Automotive OFDM Radar Systems," in *Asilomar Conf. Signals, Syst., Comput.* IEEE, 2020, pp. 1563–1567.
- [27] S. Saponara and B. Neri, "Radar sensor signal acquisition and multi-dimensional FFT processing for surveillance applications in transport systems," *IEEE Trans. Instrum. Meas.*, vol. 66, no. 4, pp. 604–615, 2017.
- [28] S. M. Patole, M. Torlak, D. Wang, and M. Ali, "Automotive radars: A review of signal processing techniques," *IEEE Signal Process. Mag.*, vol. 34, no. 2, pp. 22–35, 2017.

- [29] M. K. Samimi and T. S. Rappaport, "Statistical Channel Model with Multi-Frequency and Arbitrary Antenna Beamwidth for Millimeter-Wave Outdoor Communications," *Proc. IEEE Globecom Workshops*, 2015, pp. 1–7.
- [30] M. K. Samimi and T. S. Rappaport, "3-D Millimeter-Wave Statistical Channel Model for 5G Wireless System Design," *IEEE Trans. Microw. Theory Tech.*, vol. 64, no. 7, pp. 2207–2225, 2016.
- [31] N. WIRELESS, *Open Source Downloadable 5G Channel Simulator Software*. accessed on Aug. 2020. [Online]. Available: <http://bit.ly/1WNPpDX>
- [32] B. Lu and X. Wang, "Space-time code design in OFDM systems," In *Proc. of the IEEE Global Telecommun. Conf.*, vol. 2, 2000, pp. 1000–1004.
- [33] S. M. Alamouti, "A simple transmit diversity technique for wireless communications," *IEEE Journal on Selected Areas in Commun.*, vol. 16, no. 8, pp. 1451–1458, 1998.
- [34] V. Tarokh, N. Seshadri, and A. R. Calderbank, "Space-time codes for high data rate wireless communication: Performance criterion and code construction," *IEEE Trans. on Inf. Theory*, vol. 44, no. 2, pp. 744–765, 1998.
- [35] F. Uysal, "Phase-Coded FMCW Automotive Radar: System Design and Interference Mitigation," *IEEE Trans. Veh. Technol.*, vol. 69, no. 1, pp. 270–281, 2020.
- [36] F. Classen and H. Meyr, "Frequency synchronization algorithms for OFDM systems suitable for communication over frequency selective fading channels," *Proc. IEEE Veh. Technol. Conf.*, 1994, pp. 1655–1659.
- [37] C. Hofbauer, *Design and analysis of unique word OFDM*. Ph.D. thesis conducted at the Institute of Networked and Embedded Systems, Alpen-Adria-University Klagenfurt, Austria, 2016. [Online]. Available: <https://permalink.obvsg.at/UKL/AC12608830>
- [38] M. Huemer, J. Hausner, and H. Witschnig, "Simulation Based Optimization of Phase Tracking Algorithms for IEEE 802.11 a and Hiperlan/2 like OFDM Systems," *Proc. World Multiconf. Systemics, Cybern. Informatics*, 2002, pp. 225–229.
- [39] S. M. Kay, *Fundamentals of Statistical Signal Processing: Estimation Theory*. Prentice Hall, 1993, vol. 1.
- [40] M. Salehi and J. Proakis, "Digital communications," *McGraw-Hill Education*, vol. 31, p. 32, 2007.
- [41] M. Huemer and O. Lang, "On component-wise conditionally unbiased linear Bayesian estimation," *Proc. Asilomar Conf. Signals, Syst., Comput.*, 2014, pp. 879–885.
- [42] O. Lang, *Knowledge-Aided Methods in Estimation Theory and Adaptive Filtering*. Ph.D. thesis conducted at the Institute of Signal Processing, Johannes Kepler University Linz, Austria, 2018.
- [43] C. Hofbauer, W. Haselmayr, H.-P. Bernhard, and M. Huemer, "Impact of a Carrier Frequency Offset on Unique Word OFDM," *Proc. Int. Symp. Pers., Indoor and Mobile Radio Commun.*, London, UK, Sep. 2020, p. 7.
- [44] C. Hofbauer, W. Haselmayr, H.-P. Bernhard, and M. Huemer, "On the Inclusion and Utilization of Pilot Tones in Unique Word OFDM," *IEEE Trans. Signal Process.*, vol. 68, pp. 5504–5518, 2020.
- [45] M. Huemer, A. Onic, and C. Hofbauer, "Classical and Bayesian linear data estimators for unique word OFDM," *IEEE Trans. Signal Process.*, vol. 59, no. 12, pp. 6073–6085, 2011.
- [46] A. Viterbi, "Error bounds for convolutional codes and an asymptotically optimum decoding algorithm," *IEEE Trans. Inf. Theory*, vol. 13, no. 2, pp. 260–269, 1967.
- [47] S. Allpress, C. Lusch, and S. Felix, "Exact and approximated expressions of the log-likelihood ratio for 16-QAM signals," *Proc. Asilomar Conf. Signals, Syst., Comput.*, vol. 1, 2004, pp. 794–798.
- [48] W. Haselmayr, O. Lang, A. Springer, and M. Huemer, "Does Vector Gaussian Approximation After LMMSE Filtering Improve the LLR Quality?" *IEEE Signal Process. Letters*, vol. 24, no. 11, pp. 1676–1680, 2017.
- [49] O. Lang, M. Huemer, and C. Hofbauer, "On the log-likelihood ratio evaluation of CWCU linear and widely linear MMSE data estimators," *Proc. Asilomar Conf. Signals, Syst., Comput.*, 2016, pp. 633–637.
- [50] W. Zhang and M. J. Miller, "Baseband equivalents in digital communication system simulation," *IEEE Trans. Educ.*, vol. 35, no. 4, pp. 376–382, 1992.